Richardson, R., Whittell, G., Manners, I., Hayward, D., & Gilroy, J. (2016). An investigation into the hexagonal phases formed in high-concentration dispersions of well-defined cylindrical block copolymer micelles. *Liquid Crystals*, *43*(8), 1148-1159. https://doi.org/10.1080/02678292.2016.1170217

To appear in *Liquid Crystals*
Vol. 00, No. 00, Month 20XX, 1–15

RESEARCH ARTICLE

An Investigation into the Hexagonal Phases Formed in High-Concentration Dispersions of Well-Defined Cylindrical Block Copolymer Micelles

D.W. Hayward[a,b,c], G.R. Whittell[b], J.B. Gilroy[b,d], I. Manners[b] and R.M. Richardson[a*]

[a]*H.H. Wills Physics Laboratory, University of Bristol, Bristol BS8 1TL, U.K.*; [b]*School of Chemistry, University of Bristol, Cantock's Close, Bristol BS8 1TS, U.K.*; [c]*Bristol Centre for Functional Nanomaterials, University of Bristol, Bristol BS8 1TL, U.K.*; [d]*Department of Chemistry, The University Western Ontario, London, Ontario Canada, N6A 5B7*

(*Received 00 Month 20XX; final version received 00 Month 20XX*)

This paper presents a detailed analysis of the structure of the hexagonal phase of poly(ferrocenylsilane) (PFS)- based cylindrical micelles found at concentrations above ca. 5 wt. % in non-polar solvents such as decane. Small angle X-ray scattering indicated that the hexagonal order is not long-range. In all samples, deviations in the lower order peak positions were observed with respect to those expected for a perfect hexagonal lattice, with the degree of deviation correlating with the micelle length. Furthermore, analysis of the peak shapes and peak widths suggest that the phase possesses intermediate translational order similar to the hexatic phase. The observed features can be reproduced by amending Hosemann's paracrystal theory to include a distribution of lattice parameters to model well and poorly condensed regions. It is proposed that this distribution arises due to the bending and intertwining of individual micelles in a hexagonal lattice resulting in a kinetically-trapped phase that is initially neither perfectly hexagonal nor canonically hexatic but which anneals over time towards a perfect hexagonal lattice.

Keywords: Block Copolymer Micelles, Small-angle X-ray Scattering, Hexagonal Phase, Paracrystalline Lattice, Hexatic

1. Introduction

In the natural world, hierarchical self-assembly and self-organisation are responsible for a stunning variety of different structures and architectures.[1] Helical tropocollagen protein molecules, for example, aggregate to form fibrils which in turn come together to first form fibres and then the ever larger fibre bundles which eventually form macroscopic tendon units.[2] In order to be able to replicate or even improve upon such structures synthetically, it is necessary not only to be able to produce the constituent building blocks but also to fully understand their organisation at high concentrations and its consequences for the resulting hierarchical self-assembly.

One promising route to produce such building blocks takes advantage of the self-assembly properties of crystalline-coil block copolymers. Diblocks containing a crystallisable core-forming metalloblock such as poly(ferrocenyldimethylsilane) (PFS) for example, readily self-assemble to from 1-D cylindrical micelles in a selective solvent for the coblock.[3] Crucially, the ends of these self-assembled cylinders remain amenable to the addition of further amounts of unimer.[4] This leads to an increase in length by the epitaxial crystallization of the core-forming metalloblock that is proportional to the amount of block copolymer added, in a process known as living crystallisation-driven self-assembly (analogous to classical covalent polymerizations). It is also possible to prepare

*Corresponding author. Email: robert.richardson@bristol.ac.uk

populations of well-defined seed micelle precursors by low temperature ultrasonic fission of previously self-assembled cylinders, allowing for a high level of control over the micelle lengths.[5] Micelles produced in this way have already been shown to form lyotropic liquid crystalline phases that could be aligned in an electric field.[6, 7]

A further advantage of the block copolymer self-assembly route is the potential to carefully tune the inter-particle interactions. The chemistry of the corona can be altered by simply changing the amorphous coblock,[8] but also more subtly by cross-linking the corona,[9] quaternising the corona [10] and even adding different functionality to the corona.[11, 12] These techniques have been used to create hierarchical self-assembled structures and superstructures in solution.[13–15]

Previous work on the liquid crystalline phase behaviour of PFS-based cylindrical micelles dispersed in decane revealed the existence of nematic and hexagonal phases, however discussion of the results was focussed predominantly on the isotropic and nematic phases.[7] Indeed where the phase behaviour of semi-flexible rods has been reported elsewhere,[16–23] there has been little discussion of what occurs at high concentrations.

Previous studies of cylindrical block copolymer micelles do report the existence of a hexagonal phase occurring at high concentrations, [24–28] however in all cases where the order is discussed, this appears to be a regular, translationally well-ordered phase. Another possible phase for systems of concentrated semi-flexible rods is the hexatic, which exhibits long-range sixfold orientational order but only short range translational order. Such phases have been observed for systems of DNA molecules, [29] cationic surfactants in protic ionic liquids, [30] and *fd* virus particles. [31]

In this paper, small angle X-ray scattering (SAXS) experiments are used to probe the nature of the hexagonal phase that occurs in block copolymer micelles at high concentrations. An empirical model has been constructed to test some of the assumptions made and is compared to the measured data. A comparison of the results with those expected from other candidate phases shows that the phase exhibited by the block copolymer micelles is neither perfectly hexagonally crystalline nor canonically hexatic, although it shares features with both.

2. Experimental

2.1 *Materials*

A detailed account of the synthetic procedure is given elsewhere.[7, 32] Briefly, the poly(ferrocenyldimethylsilane)-*block*-polyisoprene (PFS-*b*-PI) diblock copolymers employed in this study were prepared by the addition of dimethylsila[1]ferrocenophane to a solution of *sec*-BuLi-initiated PI in THF before the living chains were terminated by the addition of a few drops of degassed methanol. All solvents throughout were HPLC grade, obtained from Sigma Aldrich (St Louis, MO, USA), and were passed through 0.45 μm filters prior to use.

2.2 *Sample Preparation*

Monodisperse micelles were prepared via the seeded growth method.[5] Solutions of micelle seeds were prepared by adding *n*-hexane (a selective solvent for the amorphous block and a poor solvent for the PFS block) to a vial containing a dry PFS-containing diblock copolymer. The sealed vial was then heated to 70°C for 1 hour, cooled to room temperature and allowed to age for four weeks, during which time the polymer readily self-assembles to form long rod-like micelles. Crystallite seed solutions were generated by ultra-sonication of the longer polydisperse micelles. As the ends of these seeds remain active to the addition of further unimer, micelle lengths could be tuned by adding a given amount of PFS-*b*-PI diblock copolymer (dissolved in THF) to the seed solution. An alternative self-seeding method was employed to prepare the polydisperse micelles.[33] In this case, as-grown micelle solutions were heated to a certain temperature below the melting point of the PFS block and then cooled to room temperature. This process dissolves the smallest crystalline domains of the

Table 1. Summary of micelle length distributions as determined from TEM. Adapted from [7].

Polymer	Micelle Length L_n (nm)	σ/L_n	L_w/L_n
Seeded Samples			
PFS_{53}-*b*-PI_{637}	350	0.25	1.06
PFS_{53}-*b*-PI_{637}	640	0.18	1.03
PFS_{53}-*b*-PI_{637}	1160	0.20	1.04
PFS_{53}-*b*-PI_{637}	2130	0.15	1.02
PFS_{90}-*b*-PI_{890}	805	0.18	1.03
PFS_{133}-*b*-PI_{1250}	715	0.21	1.04
PFS_{63}-*b*-PI_{1424}	495	0.17	1.03
Self-seeded Samples			
PFS_{53}-*b*-PI_{637}	700	0.70	1.49
PFS_{90}-*b*-PI_{890}	690	0.65	1.42
PFS_{63}-*b*-PI_{1424}	530	0.88	1.77

micelle fraction, making unimer available to crystallise onto the ends of the remaining fragments upon cooling. Micelle lengths and length distributions were determined via transmission electron microscopy (TEM). For each sample, a minimum of 500 micelles were measured by manually tracing the electron-rich cores visible in the micrographs using the image analysis software *ImageJ*. The results are shown in Table 1.

In order to produce samples at well-defined concentrations (10, 25, 50, 75, 100 and 150 mg/mL), large volumes of micellar stock solutions were first prepared at 0.5 mg/mL in hexane for each composition and length. Known volumes of solution were then transferred to quartz capillary tubes (Capillary Tube Supplies, Cornwall, UK) where the hexane was allowed to slowly evaporate. To prevent the micelles from drying out, a known amount of less volatile decane was added to the capillaries prior to the complete loss of hexane and the capillaries were subsequently heated at 40°C to complete the removal of the remaining hexanes. The capillaries were then sealed with epoxy resin.

2.3 *Small Angle X-ray Scattering*

The original SAXS measurements were performed at the Diamond Light Source synchrotron (Didcot, UK) on the I22 small-angle X-ray scattering instrument operating at a wavelength of 1.0 Å and a distance of 6.0 m to the Rapid-type detector. Subsequent measurements on the solvated samples were conducted using a *Ganesha* small angle X-ray scattering apparatus (SAXSLAB, Denmark) operating at a wavelength of 1.5 Å (Cu K-alpha) and a sample to detector distance of 1.4 m. The scattering patterns were detected by a Pilatus 300K X-Ray Detector (Dectris, Switzerland). The instrument was evacuated during measurements to reduce air scattering. Measurements on the dried samples were performed on beamline I911 at the MAX II synchrotron (Lund, Sweden) operating at a wavelength of 0.91 Å and a sample to detector distance of 2.9 m. The detector on this instrument was a Pilatus 1M (Dectris, Switzerland). Dectris detectors are produced in sections separated by gaps as can be seen in the images.

3. Results and Discussion

3.1 *Observations and Model*

It has previously been observed that PFS-*b*-PI micelles dispersed in decane form a translationally ordered phase at high concentrations. In azimuthally averaged data from SAXS experiments, this phase manifests as sharp Bragg reflections with scattering vectors in the ratio $1 : \sqrt{3} : \sqrt{4} : \sqrt{7}$, indicating a 2-dimensional hexagonal lattice. An attempt to determine the lattice parameter of this phase revealed a surprising effect. The positions of the lower order peaks are slightly below the values expected from the higher order peaks for a hexagonal lattice. This can be observed in Figure 1a. Note that in order to simplify subsequent modelling and also to aid comparison between different samples, the data is presented in the form of an effective structure factor, whereby the azimuthally averaged scattered intensity from the high concentration samples is divided by the azimuthally averaged scattered intensity from the corresponding low concentration samples (10 mg/mL). This is possible as at low concentrations, the contribution from inter-particle correlations is negligible and can be considered independent of scattering vector, Q. A comparison of the original datasets is given in Figure S4 and a more detailed study on the form factor of the single micelles can be found elsewhere.[7] The dashed lines in Figure 1a indicate the theoretical peak positions for a lattice parameter chosen to agree with the (100) peak and are clearly inconsistent with the higher order peaks, e.g. (210). This peak shift in the diffraction pattern can be quantified by calculating the apparent lattice parameter, a′, from each peak assuming a 2D hexagonal lattice:

$$a' = \frac{4\pi}{\sqrt{3}Q_{hk0}}\sqrt{h^2 + k^2 + hk} \tag{1}$$

It can be observed in Figure 1b and Figure 1c, that the lattice parameters from the (100) peak are 1.5-5% higher than those determined from higher order peaks. For micelles shorter than 1 μm, the micelle length is a factor in this, as it scales with the relative discrepancies (Figure 1c) and the longer micelles tend to give broader and weaker higher order peaks (Figure 2).

An analysis of the peak widths (Figure 3) revealed that, with the exception of the PFS_{63}-*b*-PI_{1424} micelles where the peak widths were commensurate with the instrumental resolution, the width of higher order reflections increases with Q. This strongly suggests that the phase in question does not have the long-range translational order of a true crystal.

In order to shed more light on the nature of the hexagonal phase, a structure factor model was constructed to reflect the observed phenomena. Simple lattice distortion models, such as the paracrystal theory of Hosemann, predict peaks that are broader and weaker at higher Q. The strength of this effect is controlled by radial and transverse lattice distortion parameters, Δr and Δt, larger values leading to broader and weaker peaks. However, such lattice distortion models always predict peak maxima at the position expected from a perfect lattice and so are unable to account for the peak shifts observed in the diffraction from the hexagonal phase.

The shifting of peaks from their expected positions in a diffraction pattern implies that different regions of the sample have hexagonal structures but with slightly different lattice parameters. Furthermore, the regions with lower lattice parameter must have a lower lattice distortion so that the Bragg peaks from these regions are more prominent at high Q. Thus a qualitative explanation of the variation in apparent lattice parameter is that the samples consist of some well crystallized regions with a smaller lattice parameter and low lattice distortion and some poorly crystallized region with a larger lattice parameter and higher lattice distortion. The apparent lattice parameter from lower order peaks would reflect an average over both types of region whereas the lattice parameter for the higher order peaks would only reflect the well crystallized regions.

The constructed model therefore consists of a normalised distribution of lattice parameters, $g(a)$, with a mean value of $\overline{a}$. To demonstrate the peak shift, we have made some reasonable, but not unique choices. For instance, for the choice of functional form for $g(a)$, we have adopted a right-

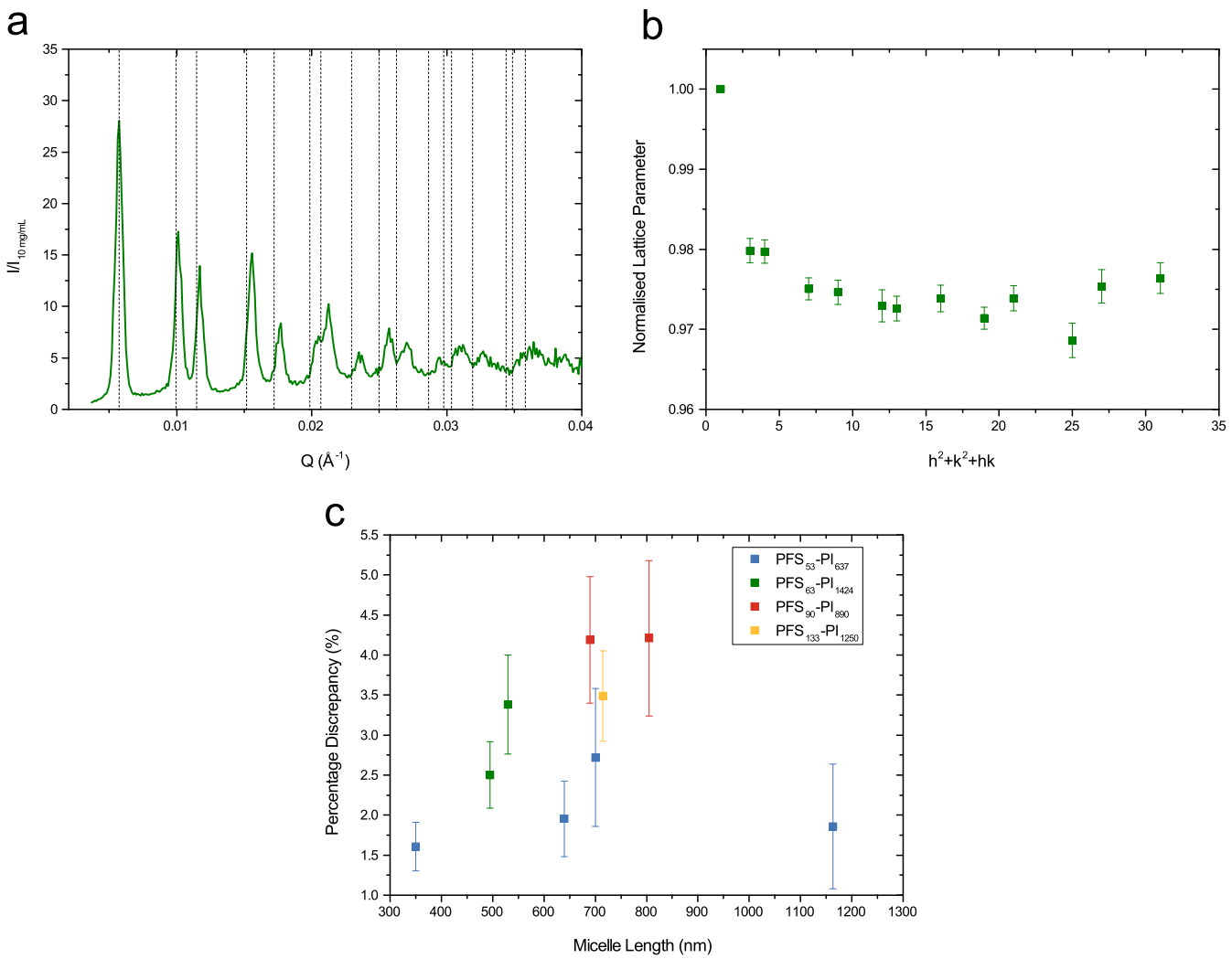

Figure 1. (a) Effective structure factor (defined as the azimuthally averaged intensity relative to that of the 10 mg/mL sample with no external field) with dashed lines indicating the theoretical peak positions for a lattice parameter chosen to agree with the (100) peak and (b) corresponding plot of the normalised lattice parameter vs $h^2 + k^2 + hk$ for 100 mg/mL decane dispersion of 530 nm long PFS_{63}-*b*-PI_{1424} micelles. (c) Plot of the average percentage discrepancy[1] vs micelle length, for all samples showing crystalline peaks.

angled triangular distribution. The lattice distortion parameters, Δr and Δt, were assumed to be proportional to the lattice parameters, raised to a power, p:

$$\Delta r = \left(\frac{a}{\overline{a}}\right)^p \Delta r_0 \tag{2}$$

The distribution of lattice parameters and corresponding behaviour of Δr are shown in Figures 4a The mean structure factor was then calculated by taking an average over the distribution of the lattice parameters:

[1] $100 \times \left(\frac{a_{(210)} - a_{(100)}}{a_{(210)}}\right)$

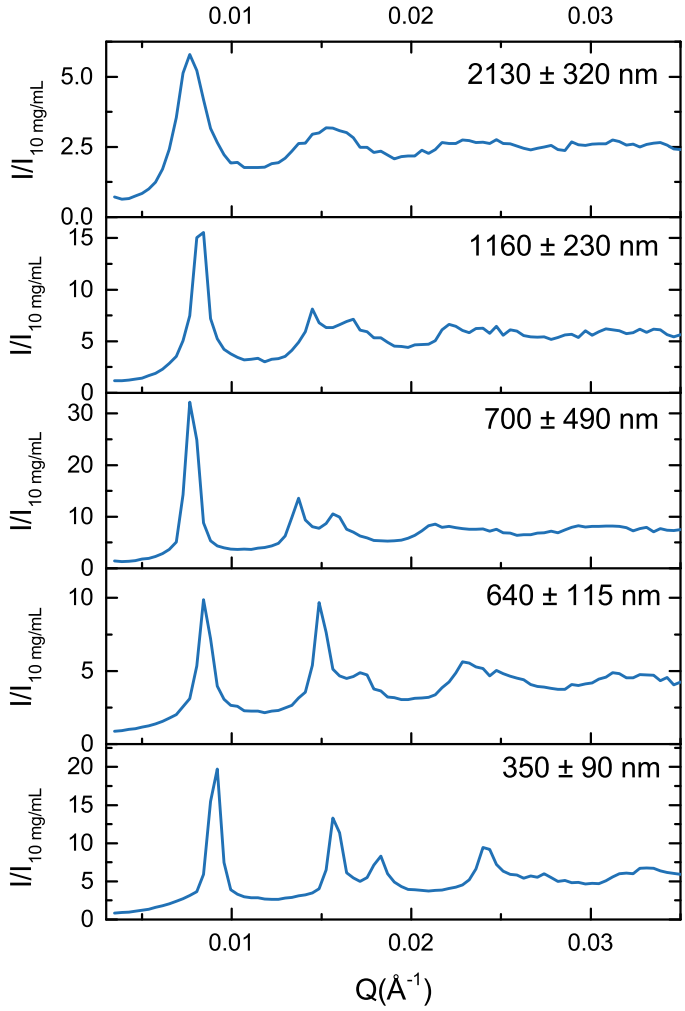

Figure 2. Plot of effective structure factor vs Q from the SAXS results of the: 350, 640, 700, 1160 and 2130 nm long PFS_{53}-*b*-PI_{637} micelles at 100 mg/mL. The effective structure factor is defined as in Figure 1. Adapted from [7].

$$S(Q) = \int g(a) S_H(Q, a, \Delta r, \Delta t)\, da \tag{3}$$

where $S_H(Q, a, \Delta r, \Delta t)$ is the structure factor for a two-dimensional hexagonal paracrystal [34–37] with lattice parameter a and distortion parameters Δr and Δt. The full model is presented in the supporting information. Again, the choice of structure factor is seen as reasonable but not unique. This model was used to fit the data and representative results are shown in Figure 4b. Although there are some discrepancies around the intensities and peak shapes, it is clear that the peaks are being shifted in the correct directions by approximately the correct amounts.

3.2 *Characterisation of Hexagonal Phase*

Given the experimental observations outlined above, the question arises as to the nature of the translational order of this phase. Although the presence and positions of the Bragg peaks imply a crystalline hexagonal symmetry, the apparent distribution of lattice parameters, lack of long range positional order and comparatively low viscosity (flow observed in capillaries) clearly suggest that the phase cannot be perfectly crystalline. For this reason, a hexatic phase has been considered.

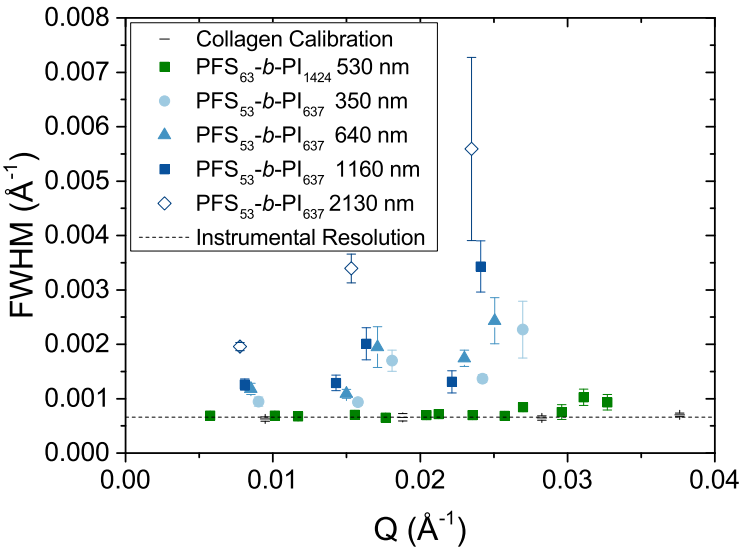

Figure 3. Peak widths from azimuthally averaged SAXS data, determined using non-linear fitting to a Gaussian distribution. All samples were at a concentration of 100 mg/mL. Filled symbols represent translationally ordered micelle phases, empty symbols represent the nematic phase. Adapted from [7].

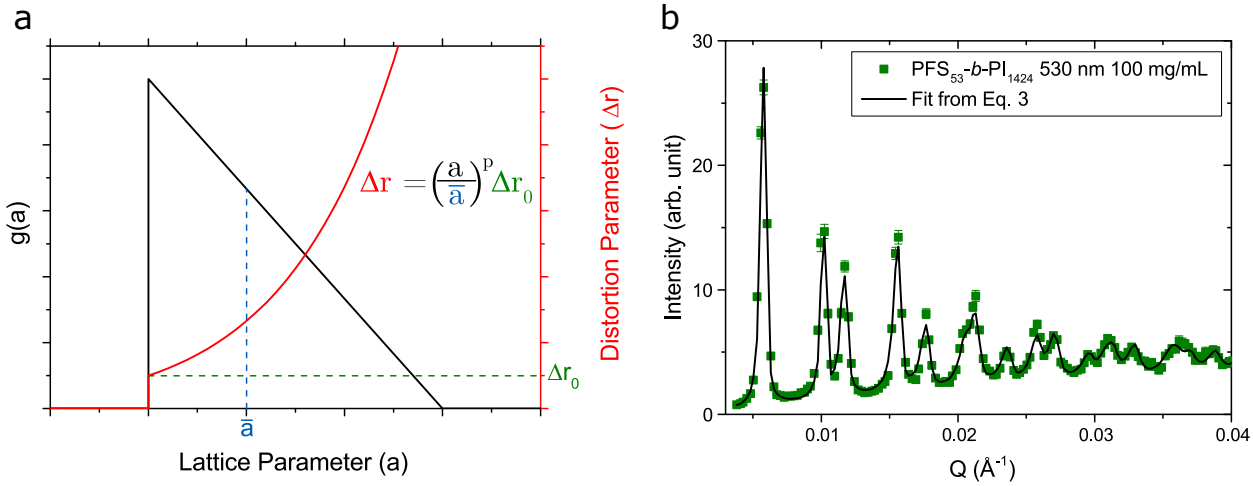

Figure 4. Plot of effective structure factor vs Q from the 530 nm PFS_{63}-b-PI_{1424} micelles at 100 mg/mL. The dashed line shows the Hosemann 2D hexagonal paracrystalline model with a distortion parameter (Eqs. 2 and 3), fitted to the experimental data.

A hexatic phase is defined by the presence of strong 6-fold orientational order but only short-range translational order due to the presence of defects, this is discussed further in section 3.3. Hexatic phases have previously been observed in lyotropic systems of amphiphilic molecules [30] and suspensions of rod-like virus particles [31] and in each case could be readily identified by the shape of the scattered intensity peaks. Whereas in conventional liquids or nematic liquid crystalline phases, the positional correlations decay exponentially with distance, leading to Lorenztian-type peak shapes, the coupling between bond orientational and positional orders in the hexatic phase give rise to square-root Lorentzian peak shapes.[38, 39] Fitting the intensity profiles along Q_z for the (100) peaks using a Pearson type VII function of the form:

$$I(Q) = \frac{I_0}{\left(\alpha\left[\xi\left\{Q - Q_0\right\}\right]^2 + 1\right)^{\kappa}} \tag{4}$$

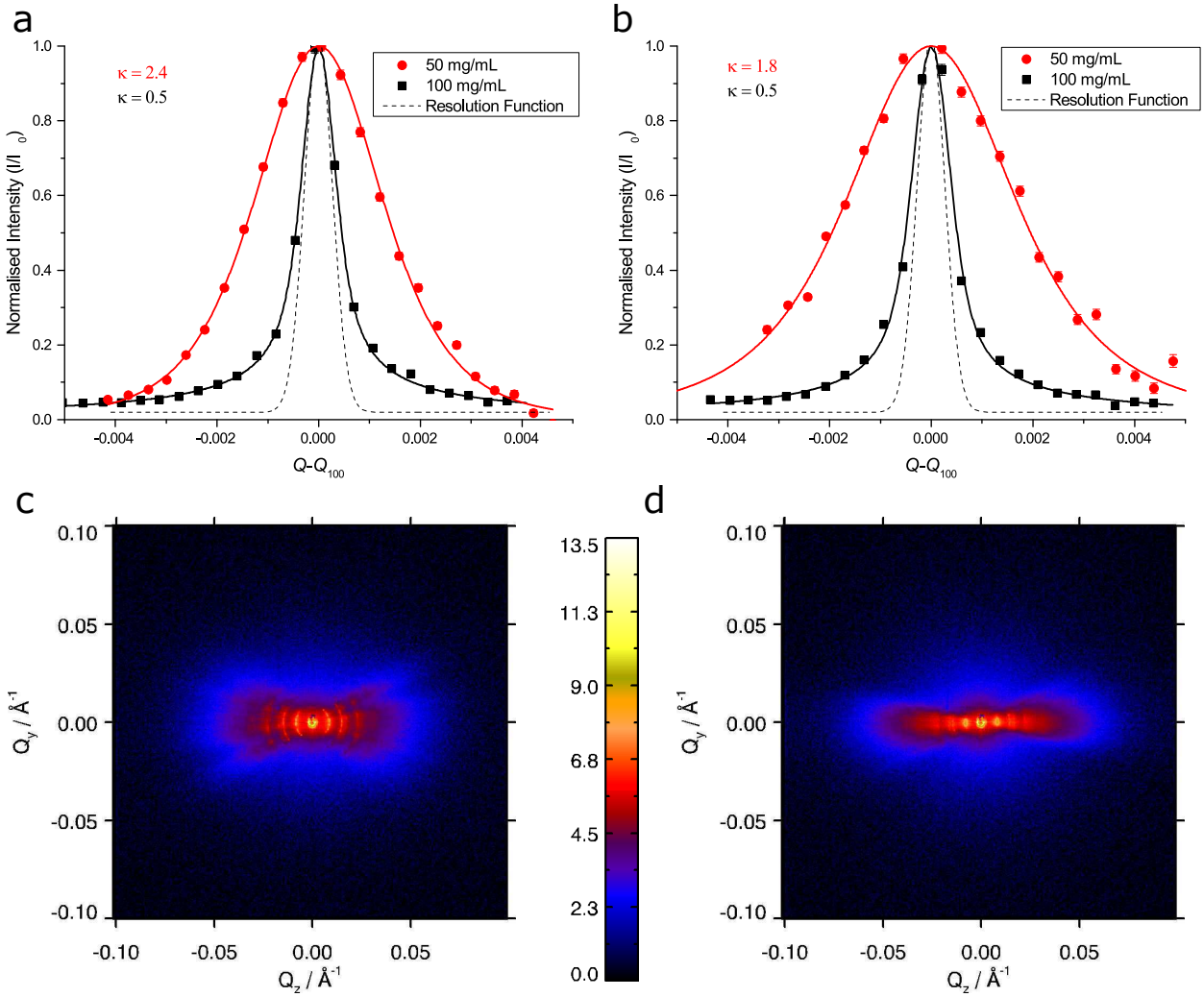

Figure 5. Azimuthally averaged intensity profile for the first peaks of the (a) 640 nm and (b) 1160 nm PFS_{53}-*b*-PI_{637} micelles. The solid lines represent fits according to Eq. 4. The data have been normalised and a linear background subtracted. Also shown are the corresponding scattering patterns for the (c) 640 nm and (d) 1160 nm samples at a concentration of 100 mg/mL.

where:

$$\alpha = \frac{2^{1/\kappa} - 1}{\pi^2} \quad \text{and} \quad \xi = \frac{2\pi}{\text{FWHM}},$$

it is possible to determine the type of peak shape. The expression reduces to a Gaussian distribution for $\kappa = -\infty$, a Lorentzian for $\kappa = 1$ and a square root Lorentzian for $\kappa = 1/2$. In order to account for the instrumental and beam resolutions, it is necessary to convolute Eq. 4 with a Gaussian distribution of fixed width (estimated from the collagen calibration samples to have a FWHM of 6.62×10^{-4} Å). A linear background subtraction and normalization have also been carried out for comparison purposes. Representative results for the 640 nm and 1160 nm PFS_{53}-*b*-PI_{637} micelles are shown in Figure 5a and 5b respectively.

The difference in peak shape between the nematic (50 mg/mL) and hexagonal (100 mg/mL) phases is stark. The 50 mg/mL peak is broad and approximately Lorentzian in character ($\kappa_{640} = 2.4 \pm 0.9, \kappa_{1160} = 1.8 \pm 1.0$) as expected from the liquid-like ordering in a nematic. The 100 mg/mL peaks are noticeably narrower with more prominent tails and are very good fits for the square-root Lorentzian distribution ($\kappa_{640} = 0.5 \pm 0.1, \kappa_{1160} = 0.5 \pm 0.09$).

It can be seen from Figures 5c and d that the micelles are aligned along the axis of the capillaries, likely due to the geometrical boundary conditions imposed during the phase transition (i.e. on

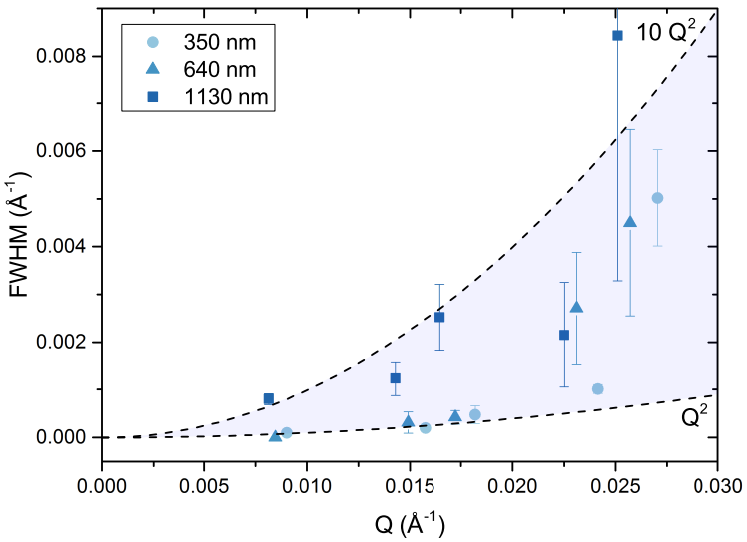

Figure 6. Plot of peak widths vs Q for PFS_{53}-b-PI_{637} micelles at a concentration of 100 mg/mL. The peak widths (full width at half maximum) were determined using non-linear regression fits to Eq. 4 convoluted with a Gaussian of fixed width. The dashed lines show a Q^2 dependence as predicted by paracrystalline theory and the envelope serves as a guide for the eye.

evaporation of the solvent). Although the scattering is not from a single macroscopic monodomain, the preferred orientation of the hexagonal domains emphasises the positional correlations from the radial inter-micelle spacing and minimises orientational averaging effects.

The peak shapes and peak widths may of course be affected by the size of the ordered domains, whereby smaller crystallites give rise to broader peaks. However, the Scherrer formula for crystallite size peak-broadening predicts an equal contribution for every peak:

$$\Delta Q = \frac{5.57}{L} \tag{5}$$

where: L is the crystallite size and ΔQ the full width at half maximum (FWHM). It can be observed from Figure 6 that the intrinsic widths increase rapidly with Q, which cannot be accounted for by the Scherrer formula. In addition, Figure 5 demonstrates that the tails of the Bragg peaks are substantially more pronounced than those of the resolution function, which is also not expected for crystallite size broadening. It is therefore clear that crystallite size is not a significant contribution to the peak widths.

Eq. 4 was also used to determine the widths of higher order peaks in the hexagonal phases and it was observed (Figure 6) that the peak widths increase rapidly with Q. This feature is typical of short-range translational order. For instance, the paracrystalline theory predicts a peak width proportional to Q^2.[40] This is consistent with the experimental results, as can be seen by the shaded envelope in (Figure 6), however it was not possible to establish the exact dependence due to the magnitude of the uncertainties. Nevertheless, this result confirms that the correlation of the micelle positions is not truly long-range, as it would be in a hexagonal crystal, but has short-range translational order (SRTO) and long-range orientational order as is characteristic of a hexatic phase. A similar analysis could not be performed for the PFS_{63}-b-PI_{1424} samples as the peak widths were essentially equal to the instrumental resolution (Figure 3).

In order to establish whether the SRTO hexagonal phase represents a true minimum in the free energy of the system (i.e. whether it exists at thermodynamic equilibrium) the original samples were allowed to age in sealed capillaries at room temperature over the course of four years and were then remeasured using SAXS. Representative results are shown in Figure 7. It can be seen that in the intervening period an annealing process has taken place that has not only dramatically reduced the discrepancies but has formed macroscopic domains at least as large as the dimensions of the

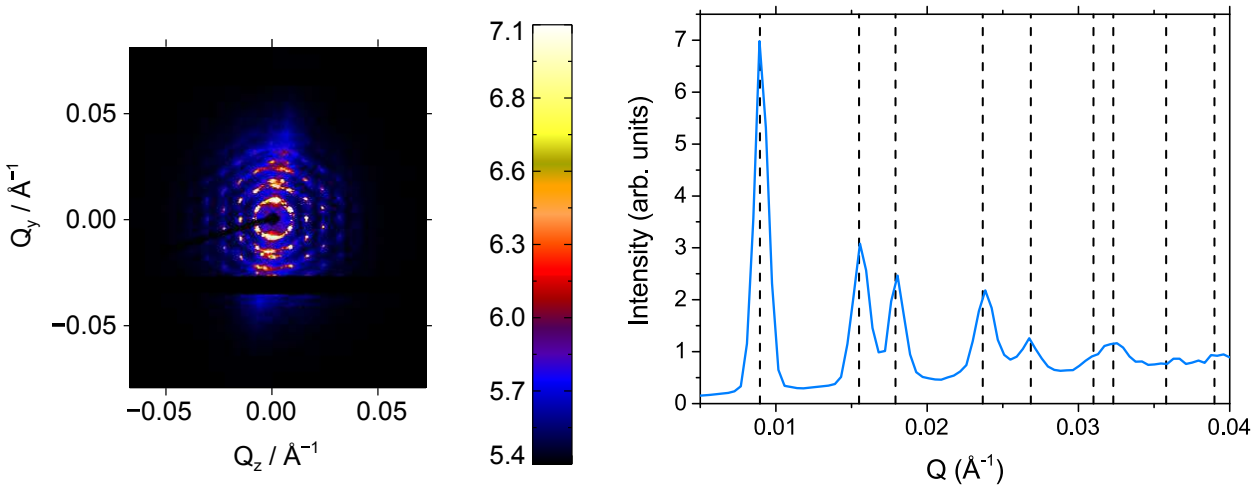

Figure 7. Scattering pattern (left) and effective structure factor (right) from self-seeded, 75 mg/mL PFS_{53}-*b*-PI_{637} micelle dispersion aged for four years.

X-ray beam (200 μm x 200 μm). The results for other samples were very similar and, although monodomains were not always visible, the average discrepancy was reduced from 3% to 0.5%. It was not possible to conduct a meaningful peak-shape or peak-width analysis, as the widths of the peaks were below the resolution of the detector, but the results do strongly suggest the appearance of long-range translational order.

The changes that occur when the concentration is increased to a maximum, on complete removal the solvent, were also examined. In this case, the capillaries containing the micelle solution were not sealed and the solvent was allowed to evaporate slowly in ambient conditions. The results, shown in Figure S5, demonstrate that the packing remains approximately hexagonal, however the peaks are much broader and less well-defined than in well-solvated micelle solutions. This is ascribed to the collapse of the amorphous polyisoprene corona interfering with the otherwise regular hexagonal packing of the micelles. As it was not possible to determine the precise concentration with any degree of accuracy and little is known about how poorly-solvated polyisoprene chains will aggregate under these conditions, it is difficult to draw any more concrete conclusions. However, it was found that when resolvated, the samples slowly returns to a more well-ordered hexagonal phase. This confirms that the structure and integrity of the micelles is not affected by the solvent concentration.

3.3 *Comparison With 'Canonical' Hexatic Phase*

The first theoretical predictions of a hexatic phase exhibiting short-range translational order but quasi long-range orientational order with sixfold symmetry were proposed to address the problem of melting in two dimensions. The theory proposed a phase transition mediated by the unbinding of topological defects, such as dislocations, resulting in an exponential decay in the translational order parameter but only an algebraic decay in the orientational order parameter.[41, 42] The theory behind hexatic phases was subsequently extended to explain the behaviour of three-dimensional, stacked liquid crystal phases, whereby the weak interaction between adjacent layers may stabilise the long-range two-dimensional orientational order within each layer.[43] This behaviour was observed in various thermotropic liquid crystal systems [44, 45] and has also been theoretically predicted for rod-like mesogens.[46] Furthermore, a continuous analogue to the stacked hexatic phase known as a 'line hexatic' has also been observed in liquid crystals composed of DNA fragments.[29]

Although they also exhibit long range orientational order with sixfold symmetry and short-range translational order, there are a number of key differences between the block copolymer micelles presented in this work and the cannonical hexatic systems outlined above. As with stacked or line

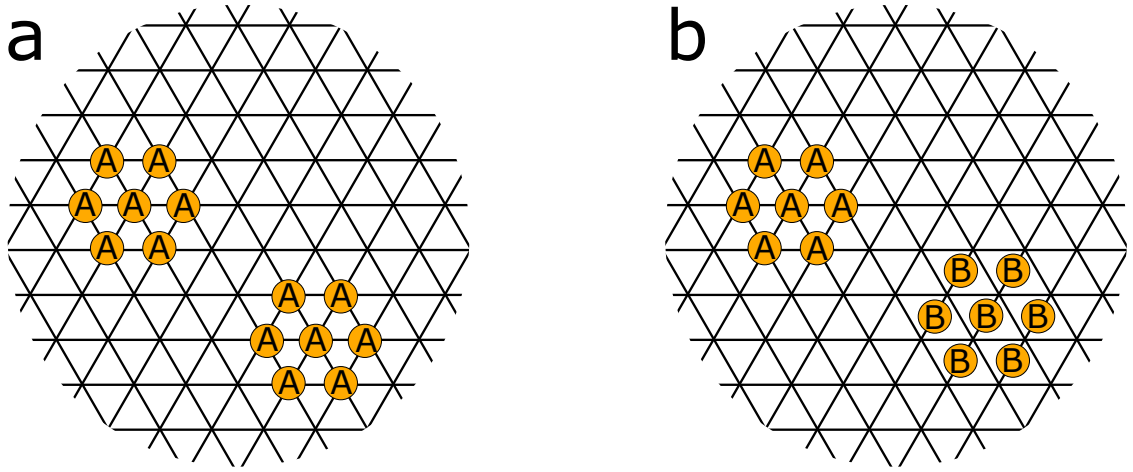

Figure 8. Classical interpretations of separated groups of mesogens in (a) a hexagonal crystal and (b) a hexatic phase. In (a) all mesogens occupy sites on the triangular lattice and therefore exhibit both long range translational as well as orientational order. In (b), although the distant groups of mesogens share the same order and orientation relative to some fixed axis, they do not occupy sites on the same lattice, giving rise to long range orientational but only short range translational order. Figure adapted from [47].

hexatic phases, systems of hexagonally packed micelles are three-dimensional, however due to the inherent flexibility of the micelles, the resulting topological defects are very different. A typical defect in a stacked hexatic is shown in Figure 8; the occupation of lattice sites varies between A and B, however the size and orientation of the unit cell remains the same. Such defects are equilibrium features of the structure, not frozen in defects that could be removed by annealing. In the case of cylindrical micelles, it is proposed that defects arise due to their inherent flexibility. As the concentration is increased, micelles will begin to cluster into a hexagonally-packed region, however, the same (or some of the same) micelles may condense into another hexagonal region but not necessarily in the same order. That is, a single micelle may occupy two different lattice points at different positions along its length and between these points there will be a poorly ordered region (Figure 9). The ultimate lowest energy configuration (i.e. at zero temperature) would be for all of the rods to be straight and parallel to minimise the bending energy, however at finite temperatures there will be an equilibrium population of crossover defects as outlined above. It is worth noting, that this behaviour is not the same as would occur in a line hexatic, where any plane drawn parallel to the local director would exhibit identical 2D hexatic order with no twisting of the mesogens.

We postulate that the initial rapid evaporation of the volatile solvent gives rise to a significant number of crossover defects in the system. As can be seen in Figure 9 these crossovers result in a range of different environments within the structure: some regions will be dense and well-ordered, others will be poorly ordered and consequently less dense, this in turn yields the distribution of lattice parameters introduced in section 3.1. With subsequent annealing over time, the number of defects decreases and the well-ordered regions dominate to form the larger monodomains seen in Figure 7. Furthermore, it is known that longer rods require less energy for a given bending angle than shorter ones. One would therefore expect more defects resulting in higher discrepancies and weaker higher-order Bragg peaks for longer micelles. This behaviour can be observed in Figures 1c and 2.

In summary, it is clear that the micelles do not form a stacked hexatic phase in the classical sense. Instead, they form an imperfect hexagonal phase which results from the rapid condensation of flexible rods. This is a transitional arrangement rather than a phase in equilibrium and the translational order improves with annealing as the flexible cylinders rearrange to minimise their bending energy and optimise the inter-micelle interactions. Ultimately, the imperfect phase anneals towards a normal 2D hexagonal phase with long range translational order and some isolated defects. In the case of the sample shown in Figure 7, this situation appears to be achieved, at least as far as can be probed with the current experimental resolution. In terms of symmetry, this phase is

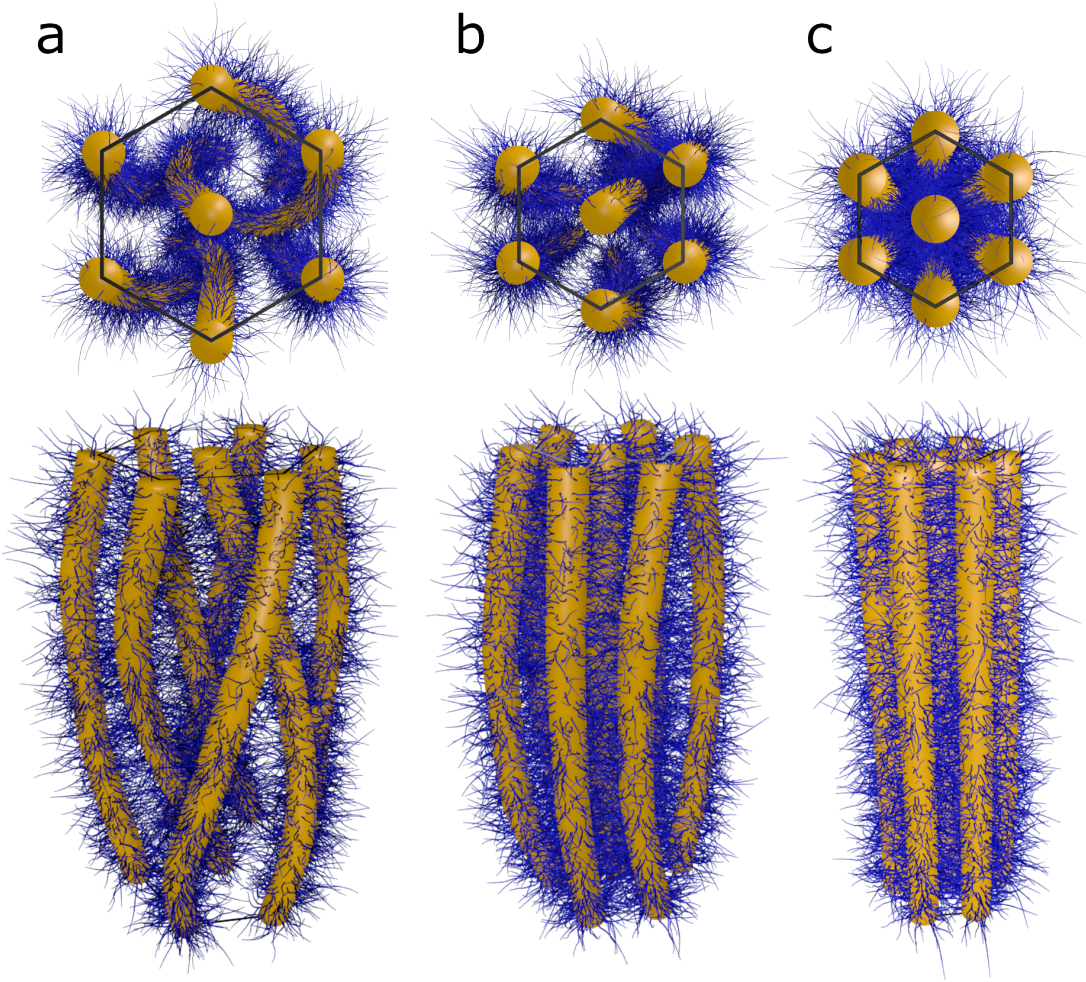

Figure 9. Schematic showing possible packing defects for flexible micelles in solution. (a) Shows both bending and intertwining defects, (b) exhibits only bending defects and (c) shows perfect hexagonal packing (i.e. no defects). As the samples anneal, the number of defects decreases resulting in smaller lattice parameters with narrower distributions.

similar to the conventional disordered columnar hexagonal $\mathrm{Col_{hd}}$, typically formed from stacks of discrete disc-shaped molecules. However, $\mathrm{Col_{hd}}$ phases composed of discs, form their equilibrium structure rapidly due to the possibility of breaking and reforming columns. In the case of continuous flexible micelles, this is not possible and the micelles are required to diffuse into their equilibrium configuration without breaking.

4. Conclusions

Small-angle X-ray scattering experiments on micellar solutions of block-copolymer micelles have revealed an, as yet unreported, hexagonal phase at high concentrations. The phase is characterised above all by a discrepancy in the positions of the first order Bragg peak with respect to the lower order peaks. Furthermore, an analysis of the peak shapes and peak widths shows that the translational order is not truly long-range. Both of these features can be accounted for if the sample is composed of regions with densely-packed well-crystallised material and regions of less dense, poorly-crystallised material. By including a distribution of lattice parameters as well as lattice distortion parameters based on Hosemann's theory of paracrystals in a model for the scattering from a two-dimensional hexagonal lattice, it was possible to accurately recreate the observed features.

The long-range six-fold orientational order coupled with the short-range orientational order de-

scribed by the data are highly reminiscent of hexatic ordering. As the samples are composed of continuous flexible cylinders and the phase in question anneals over time, it was considered unlikely to be a hexatic phase in line with canonical descriptions. Instead, it is postulated that the characteristic features occur as a result of defects caused by individual micelles bending and intertwining in a hexagonal lattice. Not only would these types of defects account for the observed range of lattice parameters, they would also be expected to anneal as the system converges on its equilibrium configuration at a finite temperature.

Although the postulated model describes the X-ray results, it would be highly desirable to observe these defects directly and follow their evolution with time. This will be the subject of future work using tomography techniques. Further exploration of this model would enhance our understanding of how systems of flexible rods interact at high concentration but also, with particular relevance to the fields of biomimetics and hierarchical self-assembly, to be able to tune such interactions using chemical functionalisation.

Acknowledgements

The authors gratefully acknowledge the Diamond Light Source and MAX-Lab synchrotron facilities for the beamtime awards (SM6035) and (20140459) and the beamline staff for their help and support.

Funding

DWH was supported by the Bristol Centre for Functional Nanomaterials under EPSRC doctoral training grant [EP/G036780/1]. JBG is grateful to the NSERC of Canada for a postdoctoral fellowship. IM thanks the European Research Council for an Advanced Investigator Grant. The Ganesha x-ray scattering apparatus used for this research was purchased under EPSRC Grant Atoms to Applications [EP/K035746/1].

Notes

The authors declare no competing financial interest.

Supplemental material

A full description of the modified Hosemann model for hexagonal paracrystals as well as an additional figure showing the phase behaviour on removal and addition of solvent, as referenced in the main text, are given in the supplementary material.

References

[1] Elemans JAAW, Rowan AE, Nolte RJM. Mastering molecular matter. Supramolecular architectures by hierarchical self-assembly. J Mater Chem. 2003;13(11):2661; doi: 10.1039/b304972h.

[2] Ottani V, Martini D, Franchi M, Ruggeri A, Raspanti M. Hierarchical structures in fibrillar collagens. Micron. 2002;33(7-8):587–596; doi: 10.1016/s0968-4328(02)00033-1.

[3] Massey JA, Temple K, Cao L, Rharbi Y, Raez J, Winnik MA, Manners I. Self-Assembly of Organometallic Block Copolymers: The Role of Crystallinity of the Core-Forming Polyferrocene Block in the Micellar Morphologies Formed by Poly(ferrocenylsilane- b -dimethylsiloxane) in n -Alkane Solvents. J Am Chem Soc. 2000;122(47):11577–11584; doi: 10.1021/ja002205d.

[4] Wang X, Guerin G, Wang H, Wang Y, Manners I, Winnik MA. Cylindrical block copolymer micelles and co-micelles of controlled length and architecture. Science. 2007;317(5838):644–7; doi: 10.1126/science.1141382.
[5] Gilroy JB, Gädt T, Whittell GR, Chabanne L, Mitchels JM, Richardson RM, Winnik MA, Manners I. Monodisperse cylindrical micelles by crystallization-driven living self-assembly. Nat Chem. 2010; 2(7):566–70; doi: 10.1038/nchem.664.
[6] Gilroy JB, Rupar PA, Whittell GR, Chabanne L, Terrill NJ, Winnik MA, Manners I, Richardson RM. Probing the structure of the crystalline core of field-aligned, monodisperse, cylindrical polyisoprene-block-polyferrocenylsilane micelles in solution using synchrotron small- and wide-angle X-ray scattering. J Am Chem Soc. 2011;133(42):17056–62; doi: 10.1021/ja207417z.
[7] Hayward DW, Gilroy JB, Rupar PA, Chabanne L, Pizzey C, Winnik MA, Whittell GR, Manners I, Richardson RM. Liquid Crystalline Phase Behavior of Well-Defined Cylindrical Block Copolymer Micelles Using Synchrotron Small-Angle X-ray Scattering. Macromolecules. 2015;48(5):1579–1591; doi: 10.1021/ma502222f.
[8] Qian J, Zhang M, Manners I, Winnik MA. Nanofiber micelles from the self-assembly of block copolymers. Trends Biotechnol. 2010;28(2):84–92; doi: 10.1016/j.tibtech.2009.11.003.
[9] Wang X, Liu K, Arsenault AC, Rider DA, Ozin GA, Winnik MA, Manners I. Shell-cross-linked cylindrical Polyisoprene-b-polyferrocenylsilane (PI-b-PFS) block copolymer micelles: one-dimensional (1D) organometallic nanocylinders. J Am Chem Soc. 2007;129(17):5630–9; doi: 10.1021/ja068730f.
[10] Wang H, Lin W, Fritz KP, Scholes GD, Winnik MA, Manners I. Cylindrical block co-micelles with spatially selective functionalization by nanoparticles. J Am Chem Soc. 2007;129(43):12924–5; doi: 10.1021/ja075587x.
[11] Lunn DJ, Boott CE, Bass KE, Shuttleworth TA, McCreanor NG, Papadouli S, Manners I. Controlled thiol-ene functionalization of polyferrocenylsilane-block- polyvinylsiloxane copolymers. Macromol Chem Phys. 2013;214:2813–2820; doi: 10.1002/macp.201300520.
[12] Hudson ZM, Lunn DJ, Winnik MA, Manners I. Colour-tunable fluorescent multiblock micelles. Nat Commun. 2014;5:1–8; doi: 10.1038/ncomms4372.
[13] Qiu H, Hudson ZM, Winnik MA, Manners I. Multidimensional hierarchical self-assembly of amphiphilic cylindrical block comicelles. Science. 2015;347(6228):1329–32; doi: 10.1126/science.1261816.
[14] Jia L, Petretic A, Molev G, Guerin G, Manners I, Winnik Ma. Hierarchical Polymer-Carbon Nanotube Hybrid Mesostructures by Crystallization-Driven Self-Assembly. ACS Nano. 2015;9(11):10673–10685; doi: 10.1021/acsnano.5b01176.
[15] Li X, Gao Y, Boott CE, Winnik MA, Manners I. Non-covalent synthesis of supermicelles with complex architectures using spatially confined hydrogen-bonding interactions. Nat Commun. 2015;6:8127; doi: 10.1038/ncomms9127.
[16] Khokhlov AR, Semenov AN. Liquid-crystalline ordering in the solution of long persistent chains. Physica A. 1981;108(2-3):546–556; doi: 10.1016/0378-4371(81)90148-5.
[17] Khokhlov AR, Semenov AN. Liquid-crystalline ordering in the solution of partially flexible macromolecules. Physica A. 1982;112A:605–614; doi: 10.1016/0378-4371(82)90199-6.
[18] Hentschke R. Equation of state for persistent-flexible liquid-crystal polymers. Comparison with poly(γ-benzyl-L-glutamate) in dimethylformamide. Macromolecules. 1990;23(4):1192–1196; doi: 10.1021/ma00206a043.
[19] Odijk T. Theory of lyotropic polymer liquid crystals. Macromolecules. 1986;19(9):2313–2329; doi: 10.1021/ma00163a001.
[20] DuPré DB, Yang S. Liquid crystalline properties of solutions of persistent polymer chains. J Chem Phys. 1991;94(1991):7466–7477; doi: 10.1063/1.460177.
[21] Chen ZY. Nematic ordering in semiflexible polymer chains. Macromolecules. 1993;26:3419–3423; doi: 10.1021/ma00065a027.
[22] Barry E, Beller D, Dogic Z. A model liquid crystalline system based on rodlike viruses with variable chirality and persistence length. Soft Matter. 2009;5(13); doi: 10.1039/b822478a.
[23] Dennison M, Dijkstra M, van Roij R. Phase Diagram and Effective Shape of Semiflexible Colloidal Rods and Biopolymers. Phys Rev Lett. 2011;106(20):208302; doi: 10.1103/PhysRevLett.106.208302.
[24] Hamley IW, Pedersen JS, Booth C, Nace VM. A Small-Angle Neutron Scattering Study of Spherical and Wormlike Micelles Formed by Poly(oxyethylene)-Based Diblock Copolymers. Langmuir. 2001; 17(20):6386–6388; doi: 10.1021/la010642f.
[25] Bouchama F, Thathagar MB, Rothenberg G, Turkenburg DH, Eiser E. Self-Assembly of a Hexago-

nal Phase of Wormlike Micelles Containing Metal Nanoclusters. Langmuir. 2004;20(2):477–483; doi: 10.1021/la035148l.

[26] Won Y. Giant Wormlike Rubber Micelles. Science. 1999;283(5404):960–963; doi: 10.1126/science.283.5404.960.

[27] Jain S, Gong X, Scriven LE, Bates FS. Disordered network state in hydrated block-copolymer surfactants. Phys Rev Lett. 2006;96(13):138304; doi: 10.1103/PhysRevLett.96.138304.

[28] Förster S, Berton B, Hentze HP, Krämer E, Antonietti M, Lindner P. Lyotropic phase morphologies of amphiphilic block copolymers. Macromolecules. 2001;34(13):4610–4623; doi: 10.1021/ma001923h.

[29] Strey H, Wang J, Podgornik R, Rupprecht A, Yu L, Parsegian V, Sirota E. Refusing to Twist: Demonstration of a Line Hexatic Phase in DNA Liquid Crystals. Phys Rev Lett. 2000;84(14):3105–3108; doi: 10.1103/PhysRevLett.84.3105.

[30] López-Barrón CR, Wagner NJ. Structural transitions of CTAB micelles in a protic ionic liquid. Langmuir. 2012;28(35):12722–30; doi: 10.1021/la302231w.

[31] Grelet E. Hexagonal Order in Crystalline and Columnar Phases of Hard Rods. Phys Rev Lett. 2008; 100(16):168301; doi: 10.1103/PhysRevLett.100.168301.

[32] Ni Y, Rulkens R, Manners I. Transition Metal-Based Polymers with Controlled Architectures: Well-Defined Poly(ferrocenylsilane) Homopolymers and Multiblock Copolymers via the Living Anionic Ring-Opening Polymerization of Silicon-Bridged [1]Ferrocenophanes. J Am Chem Soc. 1996;118(17):4102–4114; doi: 10.1021/ja953805t.

[33] Qian J, Lu Y, Chia A, Zhang M, Rupar PA, Gunari N, Walker GC, Cambridge G, He F, Guerin G, Manners I, Winnik MA. Self-seeding in one dimension: a route to uniform fiber-like nanostructures from block copolymers with a crystallizable core-forming block. ACS Nano. 2013;7(5):3754–66; doi: 10.1021/nn400124x.

[34] Hosemann R. Der ideale Parakristall und die von ihm gestreute kohärente Röntgenstrahlung. Z Phys. 1950;128(4):465–492; doi: 10.1007/bf01330029.

[35] Hosemann R. Röntgeninterferenzen an Stoffen mit flüssigkeitsstatistischen Gitterstörungen. Z Phys. 1950;128(1):1–35; doi: 10.1007/bf01339555.

[36] Hosemann R, Bagchi SN. Direct Analysis of Diffraction by Matter. Series in Physics; North-Holland Pub. Co.; 1962.

[37] Briki F, Busson B, Doucet J. Organization of microfibrils in keratin fibers studied by X-ray scattering. Biochim Biophys Acta. 1998;1429(1):57–68; doi: 10.1016/S0167-4838(98)00216-7.

[38] Aeppli G, Bruinsma R. Hexatic Order and Liquid Density Fluctuations. Phys Rev Lett. 1984; 53(22):2133–2136; doi: 10.1103/PhysRevLett.53.2133.

[39] Chou C. Multiple-Step Melting in Two-Dimensional Hexatic Liquid-Crystal Films. Science. 1998; 280(5368):1424–1426; doi: 10.1126/science.280.5368.1424.

[40] Vaĭnshteĭn BK. Diffraction of X-rays by chain molecules. Chapter 5; Amsterdam and New York: Elsevier; 1966.

[41] Halperin BI, Nelson DR. Theory of Two-Dimensional Melting. Phys Rev Lett. 1978;41(2):121–124; doi: 10.1103/PhysRevLett.41.121.

[42] Nelson DR, Halperin BI. Dislocation-mediated melting in two dimensions. Phys Rev B. 1979;19(5):2457–2484; doi: 10.1103/PhysRevB.19.2457.

[43] Birgeneau R, Litster J. Bond orientational order model for smectic B liquid crystals. J Phys Lett. 1978; 39(21):399–402; doi: 10.1051/jphyslet:019780039021039900.

[44] Nounesis G, Huang CC, Goodby JW. Thermal-Conductivity Studies near the Smectic- A -Hexatic- B Transition in a Liquid-Crystal Compound. Phys Rev Lett. 1986;56(16):1712–1715; doi: 10.1103/PhysRevLett.56.1712.

[45] Geer R, Stoebe T, Huang CC, Pindak R, Goodby JW, Cheng M, Ho JT, Hui SW. Liquid-hexatic phase transitions in single molecular layers of liquid-crystal films. Nature. 1992;355(6356):152–154; doi: 10.1038/355152a0.

[46] Martínez-Haya B, Cuetos A. Stability of nematic and smectic phases in rod-like mesogens with orientation-dependent attractive interactions. J Phys Chem B. 2007;111(28):8150–8157; doi: 10.1021/jp0715171.

[47] Chaikin PM, Lubensky TC. Principles of condensed matter physics. Cambridge: Cambridge University Press; 1995.